Influence of randomly distributed geofibers on the integrity of clay-based landfill covers: a centrifuge study

B. V. S. Viswanadham[1], S. Rajesh[2], P. V. Divya[3] and J. P. Gourc[4]

[1]*Professor, Department of Civil Engineering, Indian Institute of Technology Bombay, Powai, Mumbai 400076, India, Telephone: +91 22 2576 7344, Telefax: +91 22 2576 7302, E-mail: viswam@civil.iitb.ac.in*
[2]*Assistant Professor, Department of Civil Engineering, Indian Institute of Technology Kanpur, Kanpur-208016, India, Telephone: +91 512 259 6054; Telefax: +91 512 259 7395; E-mail: hsrajesh@iitk.ac.in (formerly research scholar, Department of Civil Engineering, Indian Institute of Technology)*
[3]*Research scholar, Department of Civil Engineering, Indian Institute of Technology Bombay, Powai, Mumbai 400076, India, Telephone: +91 22 2576 4311; Telefax: +91 22 2576 7302; E-mail: divya.nair@iitb.ac.in*
[4]*Professor, LTHE, University of Joseph-Fourier 1, Grenoble, F 38041, France, Telephone: +33 0476635134, Telefax: +33 476825014; E-mail: gourc@ujf-grenoble.fr*

Received 31 July 2010, revised 27 June 2011, accepted 28 June 2011

ABSTRACT: The main objective of this paper is to examine the influence of discrete and randomly distributed geofiber reinforcement on the integrity of clay-based landfill covers subjected to differential settlements in a geotechnical centrifuge. A series of centrifuge tests was performed on model clay-based landfill covers with and without geofiber reinforcement at 40 gravities. A hydraulic-based differential settlement simulator was used to induce continuous differential settlements with a distortion level up to 0.125. The type and moist-compacted conditions of the soil barrier and fiber content were held constant, and the thickness of the soil barrier and the fiber type are varied. The performance of the soil barrier with and without geofiber reinforcement having an overburden pressure equivalent to that of landfill covers was monitored by measuring water breakthrough at the onset of differential settlement. With an increase in the thickness of the geofiber-reinforced soil barrier, and with the provision of an overburden equivalent to that of landfill cover, the integrity of the geofiber-reinforced soil barrier was found to be retained, even after inducing a distortion level of 0.125. Analysis and interpretation of the test results indicate the significant potential for geofiber reinforcement to decrease and to retard soil crack potential in a discrete and randomly distributed soil barrier reinforced with geofibers, while retaining its hydraulic performance.

KEYWORDS: Geosynthetics, Municipal waste, Landfills, Clay barriers, Centrifuge models, Cracking, Reinforced soils, Fibers

REFERENCE: Viswanadham, B. V. S., Rajesh, S., Divya, P. V. & Gourc, J. P. (2011). Influence of randomly distributed geofibers on the integrity of clay-based landfill covers: a centrifuge study. *Geosynthetics International*, **18**, No. 5, 255–271. [http://dx.doi.org/10.1680/gein.2011.18.5.255]

1. INTRODUCTION

Despite the recent development of new municipal solid waste (MSW) treatment techniques and increased recycling rates, landfill is still the most common MSW treatment method used worldwide (Staub *et al.* 2010). The purpose of a landfill is to provide complete isolation from the surrounding environment of waste material that otherwise would pollute all the vital components of the living environment. This can be achieved by providing an impermeable barrier within waste containment systems on the top, bottom and sides of landfills. Compacted clay can be used effectively as a hydraulic barrier because of clay's low permeability, and hence such barriers are widely used wherever clay soils are abundantly available (Heerten and Koerner 2008; Camp *et al.* 2009; Gourc *et al.* 2010a).

The main challenge in using clay as a barrier material is the formation of cracks, due either to moisture fluctuations, or to the possible differential settlement of landfill

covers. The main reason for differential settlement of a landfill is ongoing biodegradation of waste. Since the cover systems are constructed on heterogeneous waste material, differential settlement can cause more damage to landfill covers than to bottom-lining systems. When the differential settlement becomes excessive, tensile cracks can be formed along the zone of sharp curvature. The most important property that affects the performance of a landfill barrier is its hydraulic conductivity. The hydraulic performance or sealing efficiency of the barrier is compromised by tension cracking, since this leads to infiltration of rainwater into the landfill, and the release of harmful gases to the atmosphere (Staub *et al.* 2011).

The deformation behavior of the soil barrier can be exemplified using the settlement ratio and the distortion level. The settlement ratio a/a_{max} is defined as the ratio of the settlement at any stage of deformation to the maximum settlement. The distortion level a/l is defined as settlement at any stage of deformation to the influence length l within which differential settlement is induced (i.e. it is measured as the horizontal length from the center of the barrier where settlement is zero or negligible). Qian *et al.* (2002) categorized the differential settlements of landfill covers into large craters having a distortion level of 0.167 (maximum strain of 1.8%) and localized depressions having a distortion level of 0.27 (maximum strain of 4.5%). As low-level radioactive wastes are stored in containers, and the spaces between these containers are filled with buffer material, there is an inevitable possibility that differential settlements may occur (Camp *et al.* 2009; Gourc *et al.* 2010a). ADEME-LIRIGM (2005) and Gourc *et al.* (2010b) reported that heterogeneous moisture content distribution in bioreactor landfills might result in differential settlement, potentially harming the integrity of the landfill cover. Keck and Seitz (2002) reported that maximum and average subsidence depth values were 3.7 m and 0.6 m at the Radioactive Waste Management Complex Subsurface Area Disposal (RWMC-SAD) site during 1983 and 2002, with distortion levels ranging from 0.066 to 0.888.

The problem of cracking of compacted clay barriers has been studied by several investigators, but studies of the deformation behavior of barriers subjected to differential settlement are very limited. It can be analyzed by full-scale testing (Edelmann *et al.* 1999; Gourc *et al.* 2010a), by reduced-scale laboratory testing (Jessberger and Stone 1991; Scherbeck and Jessberger 1993; Viswanadham and Muthukumaran 2007; Viswanadham and Rajesh 2009; Viswanadham *et al.* 2009), or by an analytical approach (Sagaseta 1987; Liang *et al.* 1994; Bredariol *et al.* 1995; Gucunski *et al.* 1996). Previous studies have shown that clay-based landfill covers are found to lose their integrity when subjected to differential settlements.

The performance of a compacted clay barrier can be improved by providing adequate overburden, by increasing its thickness, or by adding some tensile inclusions. LaGatta *et al.* (1997) reported that geosynthetic clay liners (GCLs) can be effectively used as an alternative to compacted clay barriers. The tensile strength of geotextile layers sandwiching bentonite improved the performance of a GCL. Viswanadham and Muthukumaran (2007) reported that the use of a biaxial geogrid placed within the clay barrier can limit or prevent it from cracking. The performance of a geogrid-reinforced clay barrier depends upon the selection of a suitable geogrid, and on the contact between the soil and the geogrid layer. Recently, Miller and Rifai (2004), Viswanadham *et al.* (2009, 2010b) and Gourc *et al.* (2010a) explored the use of discrete and randomly distributed fiber reinforcement (DRDF) to restrain the cracking potential of clay-based landfill cover systems. This technique was also explored earlier by Rodatz and Oltmanns (1997).

One of the main advantages of randomly distributed fibers over geosynthetic reinforcement is the absence of potential planes of weakness, parallel to the oriented reinforcement, when an adequate soil–geosynthetic interaction is not mobilized (Maher and Gray 1990; Rajesh and Viswanadham 2011). The mixing of discrete fibers with the soil is very similar to other admixtures, such as lime and cement. It has been reported that fiber reinforcement increases both the peak strength and the residual strength (Ranjan *et al.* 1994; Morel and Gourc 1997; Nataraj and McManis 1997; Santoni *et al.* 2001; Yetimoglu and Salbas 2003; Tang *et al.* 2007; Das *et al.* 2009; Park 2009; Consoli *et al.* 2010; Falorca and Pinto 2011). The tensile strength and ductility of the soil matrix have also been found to be enhanced by fiber reinforcement (Maher and Ho 1994; Ziegler *et al.* 1998; Consoli *et al.* 2011). Zornberg (2005) reported that fibers increased the friction angle between the clay barrier and a smooth geomembrane. Recently, Lovisa *et al.* (2010) reported that randomly distributed fiber inclusions introduce an apparent cohesion to the soil. Tang *et al.* (2010) reported that the interfacial shear resistance of the fiber-reinforced soil depends primarily on the rearrangement resistance of soil particles, the effective interface contact area, the fiber surface roughness and the soil composition. Viswanadham *et al.* (2009, 2010b) reported that for kaolin–sand mixture in the ratio of 4:1 reinforced with polypropylene fibers with a fiber length of 90 mm and soil fiber content of 0.5%, the coefficient of permeability was about 1×10^{-9} m/s, and increased beyond 0.5%. Recent work reported by Viswanadham *et al.* (2010b) indicated the significant influence of fibers in retarding cracking of compacted soil beams subjected to bending. However, the knowledge pertaining to the DRDF technique is very limited, particularly the influence of fiber type along with an overburden equivalent to that of landfill covers to restrain cracking of compacted soil barriers at the onset of differential settlement. Hence the motivation behind this study is primarily to use a geotechnical centrifuge to evaluate the sealing efficiency of clay-based landfill covers with and without fiber reinforcement subjected to bending conditions due to differential settlement. Figure 1 shows a schematic representation of a geofiber-reinforced soil barrier of a landfill cover. In the present study, soil barriers of two different thicknesses were modeled, and subjected to an overburden pressure equivalent to that of the closure system of low-level radioactive waste disposal and landfill sites. Polypropylene and polyester fibers with a uniform

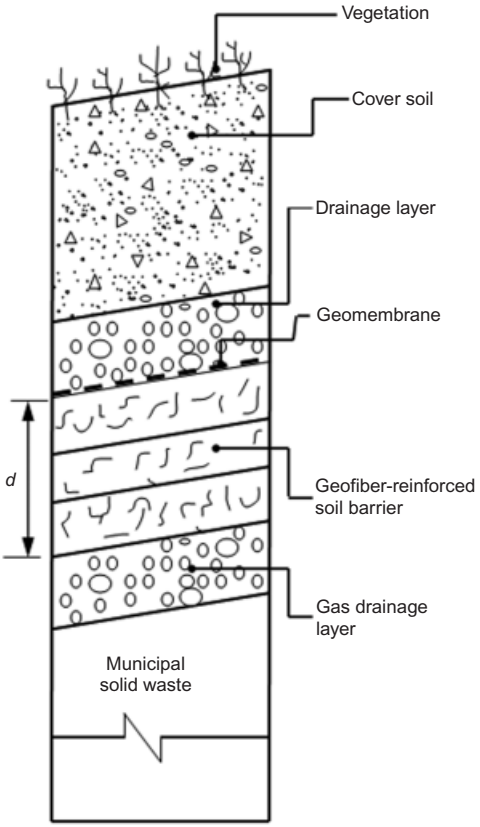

Figure 1. Schematic cross-section of landfill cover with geofiber-reinforced soil barrier

length and a fiber content of 0.5% (by dry weight of the soil) were used.

At the time of writing, to the best of the writers' knowledge, scaling considerations pertaining to the modeling of fiber-reinforced soil are limited. Only a few investigators, such as Li *et al.* (2001), Izawa *et al.* (2009) and Viswanadham *et al.* (2009) have reported results of centrifuge model tests to study the behavior of geotechnical structures involving fiber-reinforced soil.

2. CENTRIFUGE TESTS ON SOIL BARRIERS WITH AND WITHOUT GEOFIBER REINFORCEMENT

Cracking of the soil barrier and fiber–soil interaction are highly influenced by the prototype stress conditions. In small-scale modeling, the same stress levels cannot be achieved in model and prototype. Hence, in the geotechnical field, small-scale modeling does not simulate the exact field conditions. This problem can be overcome by full-scale testing, or by providing an artificial gravitational field in a centrifuge. In centrifuge testing, stress similarity is achieved by accelerating a model of scale $1/N$ to N times the earth's gravity. Here the unit weight of the model is increased by the same proportion by which the model dimensions have been reduced. In addition, the soil conditions, the loading and the response measurements can be much better controlled in the centrifuge than in full-scale testing. By considering the difficulty in performing full-scale model tests and the merits of centrifuge model tests, the centrifuge modeling technique was adopted in the present study, with the aim of studying the deformation behavior of soil barriers reinforced with randomly distributed fibers. The centrifuge tests reported herein were performed at an acceleration field of $40g$ using a 4.5 m radius beam centrifuge at the Indian Institute of Technology Bombay (IIT Bombay). The centrifuge capacity is $2500g$ kN, with a maximum payload of 25 kN at $100g$; at a higher acceleration of $200g$ the allowable payload is 6.25 kN. The detailed specifications are discussed by Viswanadham and Muthukumaran (2007).

2.1. Scaling considerations for modeling geofibers in a centrifuge

Scaling considerations of the geofibers are very important for modeling of fiber-reinforced soil in a centrifuge. In order to model geofibers in a centrifuge, the length, breadth and thickness of the geofibers have to be reduced by $1/N$ times to satisfy complete geometrical similarity between the reduced physical model and the prototype. However, it is difficult to make and use reduced dimensions for modeling geofibers in small-scale physical model tests. The most important properties of fiber-reinforced soil are the tensile strength of the fibers and the bond strength along the soil/fiber interface. Geofibers (flexible polymeric fibers) with two different cross-sections are considered for deducing scaling considerations for modeling geofibers in a centrifuge: polypropylene tape fibers with breadth b and thickness t, and very fine polyester fibers with equilateral triangular cross-section of size b.

Bond strength is important, because if perfect bonding between fibers and soil is not achieved, the fibers might be pulled out of the soil. The length of the fibers should be sufficient to achieve an adequate bond force. The crack interfaces are held together by the fibers, and thus help to reduce the cracking failure. When the first crack occurs in the soil matrix, the fiber at the point of cracking takes the entire load, and sudden extension in the fiber occurs (Taylor 1983). When fibers undergo stress within a soil–fiber composite, the force equilibrium is achieved by equating the tensile force acting perpendicular to the cross-section of the fiber and the adhesion force between the soil–fiber interfaces along the fiber length l' over the fiber surface, as shown in Figure 2. If σ_t is the tensile stress in the fiber, and τ_b is the bond stress (as shown in Figure 2), then the pullout force and tensile force for can be obtained as follows.

The pullout force is $\tau_b A'$, where $A' = 2L(b + t)$ for the rectangular cross-section and $A' = 3bL$ for the equilateral triangular cross-section. The tensile force is $\sigma_t A$, where $A = bt$ for the rectangular cross-section and $A = \sqrt{3}b^2/4$ for the equilateral triangular cross-section. The maximum pullout force can be obtained when $L = l'/2$ (considering half the length of the fiber), and the maximum tensile force can be obtained when σ_t equals the ultimate tensile strength of the geofiber, $(\sigma_t)_{max}$.

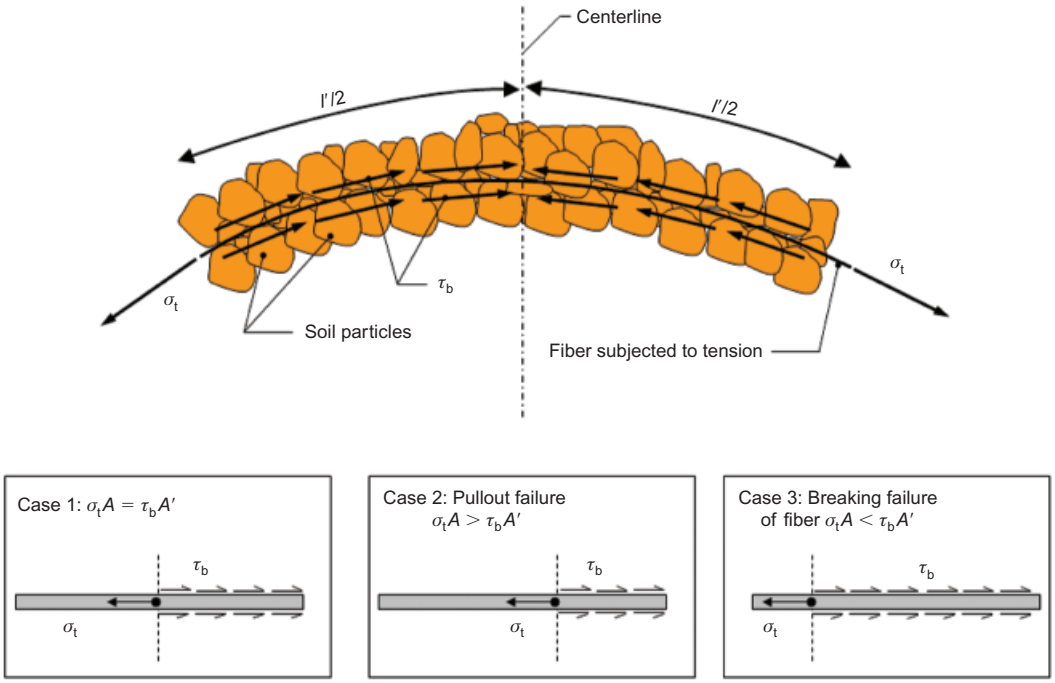

Figure 2. Schematic of soil–fiber interaction at zone of maximum curvature

The force equilibrium equation can be written as follows, for Case 1 of Figure 2.

$$\sigma_t A = \tau_b A' \tag{1}$$

After simplification, considering the maximum pullout force and maximum tensile force, Equation (1) can be written as follows.

For rectangular geofiber cross-section:

$$\frac{l'}{b} = \frac{\sigma_t t}{\tau_b (b + t)} \tag{2}$$

For equilateral triangular geofiber cross-section:

$$\frac{l'}{b} = \frac{1}{2\sqrt{3}} \frac{\sigma_t}{\tau_b} \tag{3}$$

Equations (2) and (3) lead to the scale factor of the aspect ratio as unity. The aspect ratio is defined as the ratio of length to width for fibers with a rectangular cross-section, and to the size of the side for fibers with an equilateral triangular cross-section area. However, for convenience, only fiber length was used in the present study.

Pullout or anchorage failure for geofibers with a rectangular cross-section, as shown in Case 2 of Figure 2, can occur when

$$(\sigma_t)_{\max} A > \tau_b \frac{l'}{2} 2(b + t)$$

If $(\sigma_t)_{\max} A < \tau_b (l'/2) 2(b + t)$ then two types of failure may be possible based on the location of the fiber (Cases 2 and 3): pullout failure or breakage of the fiber.

Assuming that the tensile stresses and bond stresses in the fiber with identical material characteristics in model and prototype and the constitutive law $\sigma_t = E\varepsilon_t$ (where σ_t is the tensile stress in the fiber, E is the elastic modulus of the fiber, and ε_t is the tensile strain in the fiber) and identical fiber strains in model and prototype are valid, then Equations (2) and (3) indicate that by maintaining identical aspect ratios, identical fibers can be used in the centrifuge model and the prototype. Hence the fibers can be treated as discrete inclusions and fibers with identical dimensions and properties can be used in the field. The fiber content f, which is defined as the ratio of the weight of fibers to the weight of dry soil (expressed as a percentage), can be considered as the same in the model and the prototype.

3. MATERIALS

3.1. Soil

In order to model a soil barrier in the laboratory, it is important that it should represent the barrier material properties in the field. This was achieved by analyzing the data from 85 landfills in the USA presented by Benson *et al.* (1999). Most of the soil barriers are compacted on the wet side of optimum using standard Proctor compaction energy. It was reported that, in most of the landfill sites, the soil barriers placed in the cover systems have liquid limits ranging from 30% to 40% and plasticity indices ranging from 10% to 20%. In the present study the soil barrier was modeled in such a way that it represented the above material characteristics. Various blends of commercially available kaolin and naturally available sand were tried to achieve the ideal properties, from which a kaolin–sand mix of 4:1 by dry weight was chosen as the model soil barrier material. The properties of this material are summarized in Table 1. The selected model soil is classified as CL according to the Unified Soil Classification System (USCS) and was found to be have properties

Table 1. Summary of properties of soil barrier material

Properties	Values
Hygroscopic moisture content (%)	0.9
Specific gravity	2.54
Liquid limit (%)	38
Plasticity index [%]	16
Maximum dry unit weight (standard Proctor) (kN/m^3)	15.9
Optimum moisture content (standard Proctor) (%)	22
Coefficient of permeability[a] (m/s)	0.4×10^{-9}
Shear strength parameters at 5% wet of optimum	
c' (kN/m^2)	19
ϕ' (degrees)	29
Elastic modulus of soil barrier material, E_{50} (kN/m^2)	2620

[a] Moist-compacted at maximum dry unit weight and optimum moisture content according to standard Proctor compaction.

similar to those of most of the locally available, naturally formed, fine-grained soils used for constructing soil barriers in much of India and France, and it represents the wide range of properties of the fine-grained soils used in soil barriers of landfill covers reported by Benson *et al.* (1999) and Camp *et al.* (2009). To prepare the model soil barrier, the kaolin-sand mixture was mixed and compacted at 5% wet of optimum, with a corresponding dry unit weight of 14.2 kN/m^3. The fine sand used for development of the model material in the present study was uniformly graded, and is classified as SP according to the USCS. The maximum and minimum void ratios of the sand are 0.895 and 0.597, respectively, and the corresponding unit weights are 13.57 kN/m^3 and 16.43 kN/m^3.

3.2. Geofibers

Geofibers are available in different shapes and lengths. They can be made of various material, such as polypropylene, polyester or polyvinyl alcohol, and are available in different types, such as monofilament, fibrillated, or slit-film tape. In the present study, ultraviolet-stabilized polypropylene plain tape fibers 2 mm wide and 0.02 mm thick, and polyester fibers with an equivalent diameter of 33–55 μm were used. The polyester fibers were made by polymerization of pure terephthalic acid and monoethylene glycol using a catalyst. They have a special triangular cross-section for better anchoring with other ingredients of the mix. Polyester fibers of 15 denier with tensile strength capacity of 0.6 MPa (as supplied by the manufacturer) were selected. Denier is a unit of measurement for the linear mass density of fibers; it is defined as the mass in grams of 9000 m of fiber. The tenacity is defined as the stress at which the fiber breaks, and is expressed in grams per denier (gpd). The polyester fibers were reported to have excellent acid resistance and good alkali resistance. According to Miller and Rifai (2004), the hydraulic conductivity of a fiber-reinforced clay sample remained at 1×10^{-9} m/s for a value of fiber content up to 0.5% of the dry weight of the soil sample, beyond which the hydraulic conductivity increased proportionally. The length of the fibers was selected as 90 mm, based on results reported earlier by Viswanadham *et al.* (2010b). Also, to prevent pullout failure at the zone of maximum curvature, long fibers were used in the present study. The compaction characteristics of the fiber-reinforced soil were found to have very negligible variation when compared with the soil alone. Keeping in view the results reported in the literature, a fiber content equal to 0.5% of the total dry weight of model soil (kaolin–sand mix of 4:1) was mixed uniformly. The properties of the fibers are summarized in Table 2. Polypropylene fibers have a lower specific gravity than polyester fibers. This implies a larger fiber volume, and hence the number of fibers will be greater for the same fiber content.

Table 3 summarizes the compaction and permeability characteristics of soil blended with 90 mm long polypropylene tape fibers, with fiber contents ranging from 0% (unreinforced) to 0.75%. The variations in the maximum dry unit weight and optimum moisture content are less than 5%, which is similar to the variations reported by Miller and Rifai (2004). Therefore the changes in compaction behavior of the soil due to fiber inclusion are considered insignificant. The reported values of permeability were measured by conducting falling-head tests in the laboratory at the end of three weeks' permeation time. The permeability was found to be 28 times that of the unreinforced soil for a fiber content of 0.75%. In comparison, it was observed to be only 1.25 times that of the unreinforced soil for a fiber content of 0.5%. The increase in permeability was found to be insignificant for fiber contents up to 0.5%. This implies that it is essential to limit the fiber content at or below 0.5% to achieve the

Table 2. Summary of properties of fibers used in the present study

S. no.	Properties	Polypropylene tape fibers	Polyester fibers
1	Denier	890	15
2	Specific gravity	0.91	1.334
3	Tenacity	5.45	7.0
4	Breaking load (N)	48.4	–[a]
5	Elongation strain at break (%)	18	–[a]
6	Tensile strength at break (MPa)	–[a]	0.6

[a] Not reported or not available.

Table 3. Summary of compaction and permeability characteristics of soil with and without polypropylene tape fiber reinforcement

Property	Unreinforced soil	Soil blended with 90 mm long polypropylene fibers		
		$f = 0.25\%$	$f = 0.50\%$	$f = 0.75\%$
Maximum dry unit weight (standard Proctor) (kN/m^3)	15.9	15.59	15.55	15.58
Optimum moisture content (standard Proctor) (%)	22	21.4	21.6	21.5
Coefficient of permeability[a] (m/s)	0.4×10^{-9}	7.25×10^{-10}	1.1×10^{-9}	2.5×10^{-8}

[a] Moist-compacted at maximum dry unit weight and optimum moisture content according to standard Proctor compaction.
f = fiber content.

target permeability of 1×10^{-9} m/s for soil barriers blended with polypropylene tape fibers. This observed behavior is assumed to be valid for polyester-fiber-blended soil also.

4. MODEL TEST PACKAGE, TEST PROGRAMME AND TEST PROCEDURE

A strong container with internal dimensions 720 mm length, 450 mm width and 410 mm depth was used in the present study. The container is made of well-machined mild steel plates, except for the front, which is made of thick, transparent Perspex for viewing the model during flight. A cross-section of the model test package used in the present study is shown schematically in Figure 3. By this arrangement, it was possible to model a landfill cap area as large as 520 m^2 and a central settlement of the order of 1.0 m. Friction between the walls and soil was reduced by applying a thin layer of white petroleum grease.

Differential settlements were simulated using a hydraulic-based differential settlement simulator. This comprises a hydraulic cylinder, a trapdoor settlement plate, two rigid supports, and two hinge plates with a hinge connection. The hinged aluminum plates were made to rest on the trapdoor settlement plate, connected symmetrically to the hydraulic cylinder. When the cylinder is in full stroke, a horizontal plane can be achieved, as shown in Figure 3. The model was prepared by setting the hydraulic cylinder in the full-stroke position, and an operating pressure of 400 kN/m^2 was applied. Initially, three thick nonwoven geotextile pieces overlapping one another were placed on top of the hinged doors and piston assembly to prevent the entry of coarse or fine sand

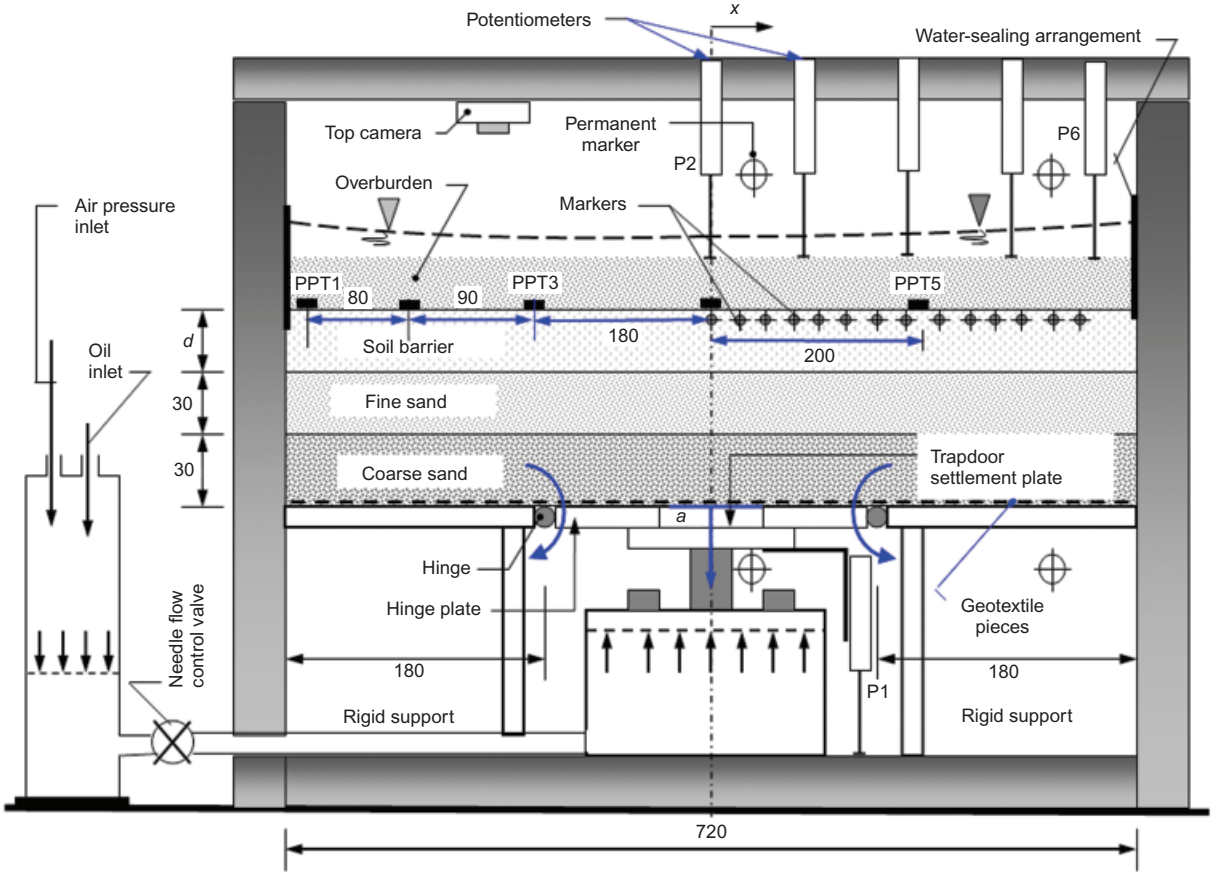

Figure 3. Cross-section of model test package (all dimensions in mm)

through gaps into the hinges, which might hinder settlement of the trapdoor. In order to prevent stress concentration near the hinges when the trapdoor settle, a sacrificial layer of coarse sand, 30 mm thick, followed by another of fine sand, also 30 mm thick, were provided before the model barrier layer was constructed. Thin filter papers were provided to act as a separator between the fine and coarse sand layers. The sand layers were presaturated and drained for about 9–10 h to facilitate compaction of the soil barriers with and without fibers to a suitable thickness. The fine sand used immediately below the soil barrier was the same as that used in preparing the model barriers. The coarse sand, which was immediately above the trapdoor settlement unit, was classified as SP according to the USCS. The peak angles of internal friction for the coarse and fine sand were found to be 43.5° and 37°, respectively, at a relative density of 55%. The main reason for using the coarse and fine sand layers below the model soil barrier was to avoid any sort of discontinuity, either in the induced settlements or in the curvature. The settling rate could be adjusted by using a needle flow control valve in the trapdoor settlement control unit. A fixed settlement rate for all the tests of 0.85 mm/min (in model dimensions) was achieved. Based on scaling considerations, the settlement rate (settlement over time) in the field, S_{rp}, is $1/N$ times the settlement rate in the centrifuge model, S_{rm}, with $t_m/t_p = 1/N^2$. This means that a settlement rate of 0.85 mm/min at $40g$ is equivalent to 30.6 mm/day in the field. This settlement rate may not be realistic when extrapolated to prototype dimensions, but to some extent these settlement rates represent localized depressions, the sudden collapse of waste containers, or ground subsidence in waste disposal sites (Keck and Seitz 2002; Qian *et al.* 2002; Gourc *et al.* 2010a).

The model barrier was moist-compacted at a moisture content of 5% wet of optimum and at a corresponding unit weight of 14.2 kN/m^3 on top of the presaturated and drained coarse and fine sand layers. The sand layers were presaturated and drained to facilitate compaction of the soil barrier to a suitable thickness. The thicknesses of the model soil barriers used in the present study were 0.6 m and 1.2 m. The model fiber-reinforced soil barrier (FRSB) was prepared in a similar way to that of the unreinforced soil barrier; the only difference was that a fiber content of 0.5% of the dry weight of the kaolin–sand mix was added. One of the difficulties in preparing FRSBs is the method used to mix the fibers into the soil. In the present study, a hand-mixing procedure was adopted to blend the soil and fibers. First, approximate proportions of dry soil were pulverized and mixed. Fibers were then weighed, and mixed gradually into the soil after mixing thoroughly with half of the desired amount of water. The remaining water was gradually mixed into the soil–fiber mix. In this way a uniform distribution of fibers throughout the specimen was achieved. The hand-mixing method will not be applicable to large-scale work in the field, though. This was used earlier by Das *et al.* (2009) and Viswanadham *et al.* (2009, 2010b).

Plastic markers were inserted along the cross-section at every 20 mm center-to-center distance and 5 mm below the top surface of the model barrier to measure the displacements of these markers during various stages of the test. A 10 mm square grid of markers was also placed on the top surface of the model soil barrier surface along the zone of maximum curvature (i.e. along the hinge axis, which is an axis showing the position of the mechanical hinge that connects the side box and the trapdoor settlement plate, as shown in Figure 3). Figures 4a and 4b show a front view and a top view of the model barrier before placing the overburden.

Instrumentation of the model soil barrier involves mainly the placement of potentiometers, to monitor the deformation profiles of the soil barrier surface and trapdoor settlement plate, and pore pressure transducers (PPTs). Five PPTs (Type PDCR81, manufactured by Druck Limited, UK) were placed above the properly prepared soil barrier surface, as shown in Figure 3, to monitor the water level and determine the water breakthrough and limiting distortion level at which the soil barrier with and without fibers loses integrity. In order to prevent leakage of water between the sides of the container and the soil barrier, a watertight seal made of a thick

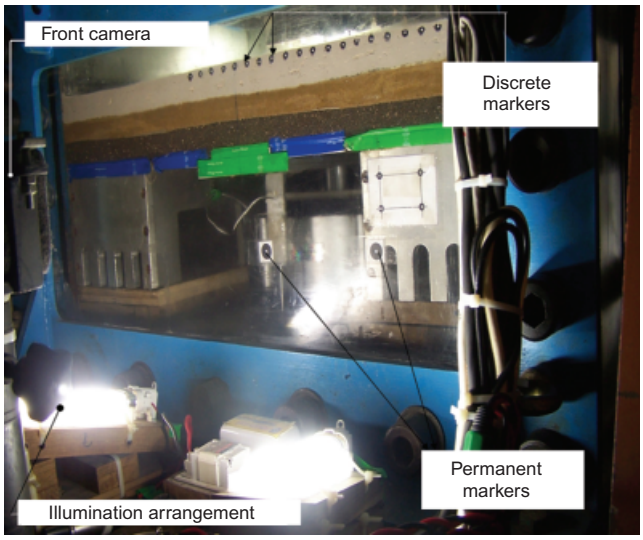

(a)

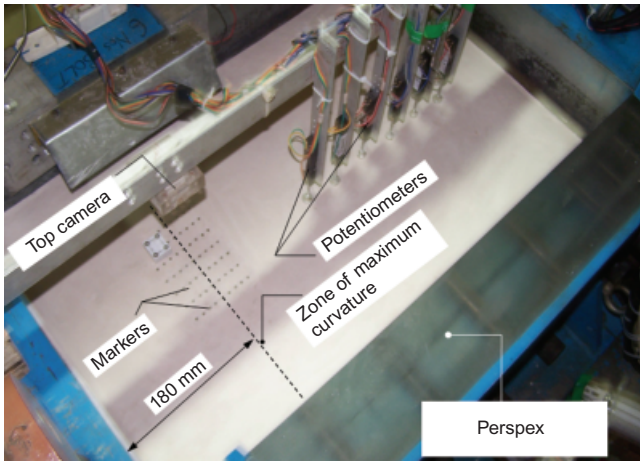

(b)

Figure 4. (a) Front elevation of a model test package and (b) top view of model soil barrier surface before centrifuge test

bentonite paste was applied all along the sides of the soil barrier. To achieve an overburden pressure of 25 kN/m^2, a sand layer, 27 mm thick, was pluviated to achieve a relative density of 55%, above which a calculated quantity of water was added so that it formed 10 mm of free-standing water. During the centrifuge test, the pressure generated by the water may be lost once water starts to infiltrate through cracks. In addition to the above, one potentiometer was attached to the trapdoor plate to monitor its movement, which would provide the central settlement a values starting from zero to a maximum of 25 mm in model dimensions during the centrifuge test. In prototype dimensions this represents a settlement value of 1 m.

After placing all the soil layers and connecting all the PPTs and potentiometers to an onboard data acquisition system, the centrifuge was set directly to 40g acceleration by rotating at a constant angular velocity of 93 rev/min and waited for about 10 min to establish equilibrium of the entire system. After completing the waiting period, the air pressure within the oil tank was slowly reduced in steps, to maintain a constant rate of settlement of the trapdoor–cylinder assembly. The top camera and front camera helped in capturing pictures showing the propagation of cracks at the zone of maximum curvature at the onset of differential settlement. However, as the topmost surface of the barriers was hidden by the sand overburden layer, the view of the model soil barrier surface could not be monitored during the centrifuge test. At various stages of central settlement, photographs of the front elevation of the model were taken using image-acquisition software, and were later used for image analysis to compute deformation profiles and the strain distribution along the surface of the soil barrier. If the induced central settlement is equal to 25 mm, or central settlement was achieved during the penultimate stages of centrifuge test, whichever is the greater is referred as the maximum central settlement a_{max}. In order to induce $a_{max} = 25$ mm at 40g for all the tests, a mechanical stopper was placed to prevent a central settlement of more than 25 mm. The distortion level can be determined using the ratio of the central settlement at any stage of deformation, a, to the influence length l within which differential settlement is induced (as shown in Figure 3). The length l is defined as the horizontal distance between the mid-span of the soil barrier and 20 mm away from the hinge axis, where deformations reduce to zero, or are very negligible: that is, 200 mm and 8 m (at 40g) from the mid-span in model dimensions and prototype dimensions, respectively. This was decided based on experience obtained from a number of tests conducted using a hydraulic-based differential settlement simulator. At the end of the centrifuge test, the model was taken out of the centrifuge chamber, and post-test analyses were performed, such as calculating the amount of water retained, tracing the cracking pattern on the surface, and crack propagation along the cross-section of the soil barrier. Table 4 provides details of the various centrifuge tests reported in this paper. Details of unreinforced model BFL8 have already been discussed by Viswanadham and Rajesh (2009).

5. ANALYSIS OF CENTRIFUGE TEST RESULTS

The influence of discrete and randomly distributed fiber inclusions on the deformation behavior of soil barriers subjected to differential settlements was evaluated with the help of the water breakthrough, strain distribution and limiting distortion level at the onset of breakthrough. Table 5 summarizes the results of the centrifuge tests conducted to evaluate the influence of discrete fiber reinforcement on the integrity of clay-based landfill covers when subjected to differential settlements.

5.1. Deformation behavior

The deformation profiles of the top surface of the soil barrier for various stages of central settlement were obtained from the measured potentiometer data and image analysis of the discrete markers embedded along the right-hand side of the soil barrier (Figure 3). Potentiometers were placed at a spacing of 100 mm center to center from the center of the barrier. High-resolution pictures of the front elevation of the model, captured at various stages of the central settlement, were used for digital image analysis using GRAM++ software (GRAM++ 2004). Variation of the actual movement of the discrete markers with reference to zero central settlement was determined at every stage of central settlement. Four permanent markers,

Table 4. Details of centrifuge tests

Sr. no	Test	g level	d (mm)	Fiber type	Fiber content, f (%)	Fiber length, l' (mm)	σ_o (kN/m^2)	a_{max} (mm)
1	BFL5r	40	30 (1200)	–[b]	–[b]	–[b]	25	25 (1000)
2	BFL8[a]	40	15 (600)	–[b]	–[b]	–[b]	25	25 (1000)
3	BFL4A	20	30 (600)	PP	0.5	90	12.5	25 (500)
4	BFL4B	40	30 (1200)	PP	0.5	90	25	25 (1000)
5	BFL4C	40	30 (1200)	PET	0.5	90	25	25 (1000)
6	BFL4D	40	15 (600)	PET	0.5	90	25	25 (1000)

[a] After Viswanadham and Rajesh (2009).
[b] Not relevant.
d = thickness of soil barrier; f = fiber content; l' = fiber length; σ_o = overburden pressure; a_{max} = maximum central settlement.
Prototype values are given in parentheses.

Table 5. Summary of centrifuge test results

Parameter	Test					
	BFL5r	BFL8	BFL4A[c]	BFL4B	BFL4C	BFL4D
Thickness of soil barrier, d (mm)	30 (1200)	15 (600)[a]	30 (600)	30 (1200)	30 (1200)	15 (600)
Type of soil barrier tested	UR	UR	PP-FR	PP-FR	PET-FR	PET-FR
Overburden pressure, σ_o (kN/m2)	25	25	12.5	25	25	25
Maximum central settlement, a_{max} (mm)	25 (1000)	25 (1000)	25 (500)	25 (1000)	25 (1000)	25 (1000)
Nature of failure	Full-depth cracking	Full-depth cracking	Tiny surface cracks	Tiny surface cracks	Tiny surface cracks	Narrow and deep cracks
Limiting distortion level, (a/l)lim	0.083	0.069	0.107	0.115	0.119	0.081
Maximum outer fiber strain (%)[b]	3.72	2.7	1.81	3.18	3.94	2.87

[a] Prototype values are indicated within parentheses.
[b] At a_{max}.
[c] At 20g only.
UR = unreinforced; PP-FR = reinforced with polypropylene fibers; PET-FR = reinforced with polyester fibers.

whose coordinates were predefined, were fixed on the inner side of the Perspex, as shown in Figures 3 and 4a. The coordinates of the discrete markers were determined with reference to the coordinates of the permanent markers using the map edit module of GRAM++. A deformation profile was fitted for different marker positions at various central settlement values, and it was found to match the exponential equation of the normal distribution (Sengupta 2005). Only the right-hand portion of the model soil barrier was shown, because of symmetry. When the horizontal distance from center of the soil barrier, x, is zero (Figure 3), the value of settlement is defined as the central settlement, which is represented as a. Figures 5a and 5b show the deformation profiles of the soil barrier surface for soil barriers with and without fiber reinforcement. Measured potentiometer data are also plotted in Figures 5a and 5b. This shows good agreement between the measured potentiometer data and the deformation profiles obtained from image analysis of the markers.

5.2. Strain variation

The shape of the deformed barrier is given by the deformation profile $w(x)$, where x is the horizontal distance from the center of the model soil barrier. By differentiating $w(x)$ successively, the respective slope and curvature can be obtained. Simple beam theory was assumed to be valid when computing strains from the deformation profiles. The strains were computed using a combined bending and elongation method (Lee and Shen 1969; Scherbeck and Jessberger 1993; Tognon *et al.* 2000). The detailed methodology adopted for computing deformation profiles and strains was explained earlier by Viswanadham and Rajesh (2009). The equation for obtaining the strain distribution from the center of the soil barrier (i.e. $x = 0$) along the top surface of the soil barrier, due to elongation and bending, is

$$\varepsilon(x) = \varepsilon_{\Delta l}(x) \pm \varepsilon_{\kappa}(x) \tag{4}$$

where $\varepsilon(x)$ is the outer fiber strain along the top surface of the soil barrier due to both elongation and bending; $\varepsilon_{\Delta l}$ is the strain due to the change in length along the length of the barrier; and $\varepsilon_{\kappa}(x)$ is the strain due to change in the curvature of the soil barrier.

The variation of the outer fiber strain distribution for the unreinforced and fiber-reinforced models along the horizontal distance from the center of the barrier are shown in Figure 6. Here the tensile strains are plotted as positive. It can be seen that, as the central settlement increases, the strain values also increase. There is a definite trend of a change in strain from tensile to compressive near 2 m distance from the centerline of the barrier. The maximum outer fiber tensile strains were found to develop near the hinge line, which is at a distance of 7.2 m from center. When the strain value increases beyond the permissible value of the barrier material, then cracks may occur and propagate, which can affect the functionality of the cover system.

6. RESULTS AND DISCUSSION

The performance of the soil barriers with and without fibers at the onset of differential settlement was analyzed using a centrifuge technique at 40g. Controlled deformations were induced by lowering the trapdoor–cylinder system below the model barrier. Differential settlement can be characterized either by the settlement ratio or by the distortion level. For the developed test package configuration, a distortion level a/l (i.e. a_{max}/l) up to 0.125 could be imposed on the barrier during centrifuge tests.

Comparisons were made in terms of outer fiber strains, the radius at the zone of maximum curvature, and the infiltration ratio for all model barriers at various distortion levels. From the outer fiber strain distributions along the horizontal distance from the center of the barrier, as shown in Figure 6, the maximum outer fiber strain corresponding to each central settlement can be obtained. The values of maximum outer fiber strain were plotted against settlement ratios and distortion levels for all the model barriers, as shown in Figure 7. The maximum outer fiber strain was found to increase for all the model barriers as the distortion level increased. It can also be seen that, up to a certain settlement ratio and distortion level, the variation of the maximum outer fiber strain with

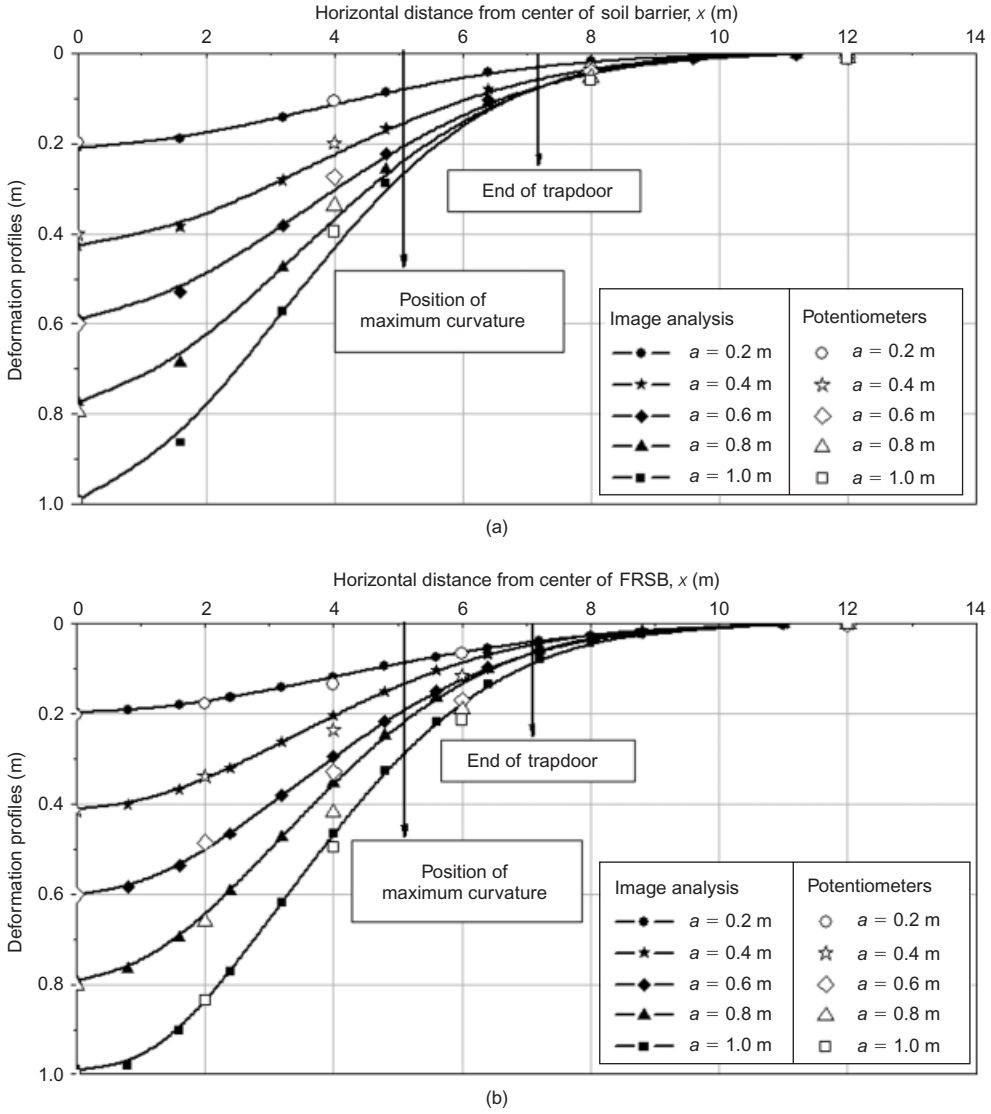

Figure 5. Deformation profiles: (a) unreinforced soil barrier (Model BFL8); (b) geofiber-reinforced soil barrier (Model BFL4D)

settlement ratio has a gentle slope, but thereafter the slope is considerably steeper. This variation can be seen in all the model barriers of identical thickness, both with and without geofiber reinforcement.

The curvature of the deformed soil barrier, $\kappa(x)$, is the second derivative of the deformation profile of the soil barrier, $w(x)$. The reciprocal of the curvature is the radius R of the deformed barrier at a distance x from the center of the soil barrier. The radius and the curvature for all the model soil barriers were determined for settlement ratios from 0 to 1 at 0.2 intervals. The variation of the maximum outer fiber strain was plotted against the radius at the maximum curvature on a semi-log scale, as shown in Figure 8. Irrespective of the barrier type, identical response of barriers to the artificially induced differential settlements could be obtained for identical thickness. This also shows the efficient functionality of a differential settlement simulator in inducing the continuous differential settlements used in the present study.

The efficiency of a barrier as an effective sealing layer can be understood from the reduction in the known volume of water stored above the barrier surface. This can be determined from the change in water level or the height of water measured using PPTs, which are installed at the top surface of barrier placed at the mid-width of the container (Figure 3). Water tends to accumulate in the central portion of the barrier as it deforms owing to the induced central settlements. The initial height of the water present above every PPT was measured before the commencement of inducing movement in the central platform. The volume per unit width of water was obtained by numerical integration of the area under the measured water profile. The height of the water along the width of the container was taken as identical to the measured value at the mid-width of the container. The total volume of water above the soil barrier is twice the volume of water computed for one half section, which is the product of the volume per unit width of water and the width of the container. The ratio of the numerical difference between the initial volume of water V_0 and the volume of water at any instant (V_a) to V_0 is defined as the infiltration ratio. This ranges from 0 to 1, corresponding to no flow to complete flow of water through the soil barrier. The variation of infiltration ratio with various settlement ratios

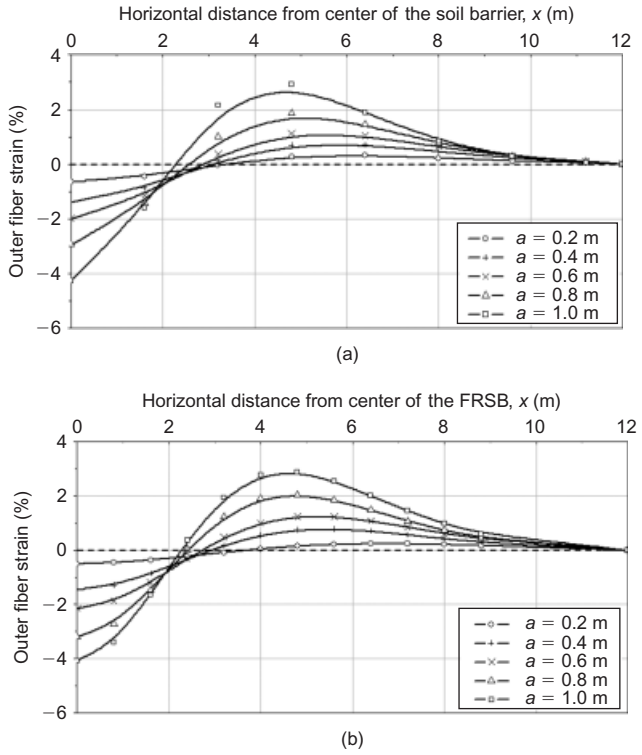

Figure 6. Variation of outer fiber strain with horizontal distance from center of soil barrier: (a) unreinforced soil barrier (Model BFL8); (b) geofiber-reinforced soil barrier (Model BFL4D)

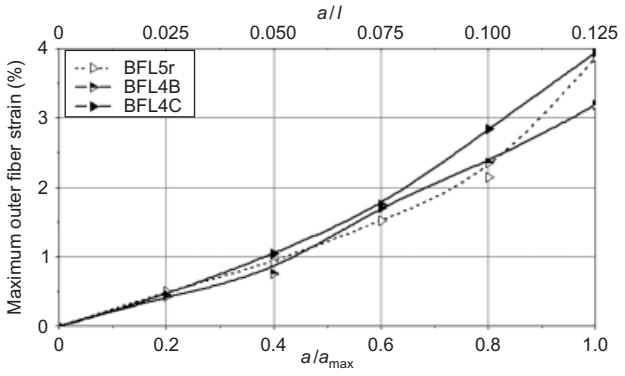

Figure 7. Variation of maximum outer fiber strain with a/a_{max} and a/l ($d = 1.2$ m)

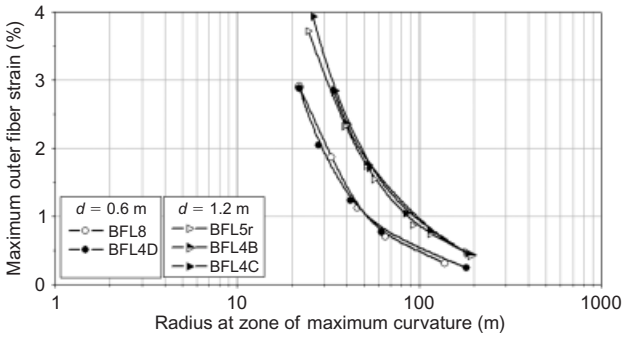

Figure 8. Variation of maximum outer fiber strain with radius at zone of maximum curvature

and distortion levels for all the model barriers is shown in Figures 9a and 9b. The distortion level corresponding to water breakthrough is termed the limiting distortion level, $(a/l)_{lim}$. It can be determined by the back-tangent method. In Figures 9a and 9b, the magnitudes of central settlement at which a considerable increase occurs in the value of the infiltration ratio are presented. Viswanadham *et al.* (2010a) carried out simple beam tests to evaluate the flexural behavior of soil beams made out of moist-compacted, fine-grained soils. The soil beams were made of a kaolin–sand mix in a 4:1 ratio, which is the same as the model material adopted in the present study. Viswanadham *et al.* (2010a) reported that the model soil barrier material compacted at its maximum dry unit weight and optimum moisture content (standard Proctor compaction) had a tensile strain at initiation of cracking of 0.99%. For the same soil, when the molding water content was increased (OMC + 4%), the strain at crack initiation was found to be 1.09%. This implies that once the outer fiber strain attains the value of a strain at crack initiation, cracking within the soil barrier might have initiated during the centrifuge test. In the present centrifuge study, owing to the presence of sand as an overburden, the exact distortion level corresponding to crack initiation of the soil barrier with and without fiber inclusions could not be ascertained. However, as the cracks extend to sufficient width and depth, the initiation of water flow through cracks can be determined from the increase in the infiltration ratio. From post-test examinations of deformed soil barriers, it was confirmed that there was no side leakage for all the models. Hence the reduction in water volume can only be due to infiltration of the water, either through pore spaces present in the soil barrier, or through cracks.

Tables 4 and 5 give particulars and results of centrifuge model BFL4A reinforced with 90 mm long polypropylene fibers (PP-FR) with a fiber content of 0.5%. However, owing to some equipment restrictions on the day of testing this model, only 20g could be maintained. In view of this, the thickness of the soil barrier is 0.6 m and $a_{max} = 0.5$ m, with an overburden equivalent to 12.5 kPa only (in prototype dimensions).

6.1. Influence of geofiber reinforcement

Model BFL5r was unreinforced (UR), and models BFL4B and BFL4C were reinforced with polypropylene (PP-FR) and polyester (PET-FR) fibers respectively (Table 4). As shown in Figure 8, as the distortion level increases, the maximum outer fiber strain of all barriers increases, regardless of the nature of the soil barrier (UR/FR) or type of fiber (PP/PET). The maximum outer fiber strain at a distortion level of 0.125 was found to be 2.7% and 3.8% for 0.6 m thick (Model BFL 8) and 1.2 m thick (Model BFL5r) unreinforced soil barriers, respectively. LaGatta *et al.* (1997) reported that tensile strains at failure of compacted soil barriers typically range from 0.1% to 4%. The maximum outer fiber strain for the 1.2 m thick barrier was 25–30% more than for the 0.6 m thick barrier. The distortion level corresponding to water breakthrough (i.e. $(a/l)_{lim}$) was found to be

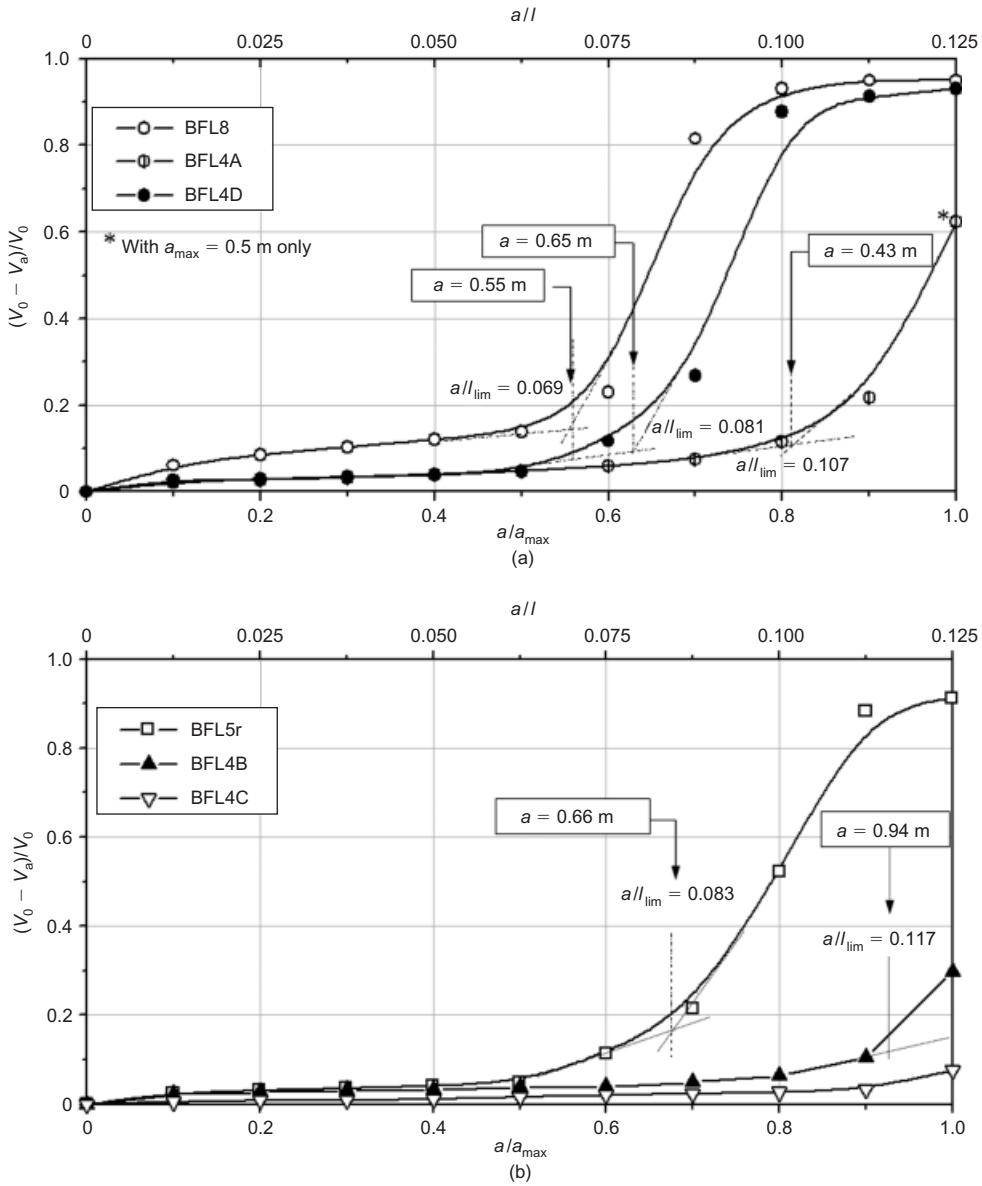

Figure 9. Variation of infiltration ratio with a/a_{max} and a/l: (a) $d = 0.6$ m; (b) $d = 1.2$ m

0.069 for the 0.6 m thick barrier (Model BFL8) and 0.083 for the 1.2 m thick barrier (Model BFL5r). Hence it is clear that the thick soil barrier can withstand greater deformation; however, the thickness of the unreinforced soil barrier is not sufficient to sustain a distortion level of the order of 0.125. As shown in Figure 8, identical responses of the barriers to the artificially induced differential settlements could be obtained for identical thickness of soil barriers, regardless of the barrier type (UR/FR) or fiber type (PP/PET). Significant shift in the curves can be observed for the thin and thick soil barriers. A similar trend was reported by Viswanadham and Muthukumaran (2007) and Viswanadham and Rajesh (2009) based on centrifuge tests on moist-compacted soil barriers with and without geogrid inclusion, using a hydraulic-based differential settlement simulator.

When the cracks extend to sufficient width and depth, water has a tendency to flow through the barrier, and the infiltration ratio increases. As can be noted from Figure 9a, the values of infiltration ratio were found to be on the higher side for 0.6 m thick unreinforced soil barrier when compared with the polyester-fiber-reinforced barrier for the entire range of distortion level from 0 to 0.125. The value of the limiting distortion level for a 0.6 m thick polyester-fiber-reinforced barrier was found to be 1.75 times greater than for a 0.6 m thick soil barrier without any fibers. This indicates the influence of fibers in maintaining sealing efficiency and retarding water breakthrough in the soil barrier at the onset of differential settlement. The limiting distortion level of a 0.6 m thick soil barrier reinforced with polypropylene fibers with a maximum central settlement of 0.5 m was found to be 0.107. The magnitude of central settlement at which a water breakthrough was observed for model BFL4A observed was found to be slightly less than for the unreinforced case (Figure 9a). The significant influence of the inclusion of polypropylene fibers on the integrity of the 0.6 m thick soil barrier could not be registered, mainly because of the lower overburden pressure (12.5 kPa). The influence of the thickness of the soil barrier on the

deformation behavior of FRSBs can be clearly seen from a slight delay in water breakthrough, and by a relatively higher distortion level being sustained. The variation of the 0.6 m thick barrier reinforced with polyester fiber was found to be comparable with the variation of the 1.2 m thick unreinforced soil barrier. This suggests a possible reduction in the thickness of the soil barrier upon inclusion of geofibers. The values of the limiting distortion level for a 1.2 m thick soil barrier with polypropylene and polyester fibers with a fiber content of 0.5% (Models BFL4B and BFL4C) were registered as 0.117 and 0.119, respectively. In both models, 50% of the initial volume of water stored on the soil barrier could be collected immediately after completion of the centrifuge tests. Moreover, during all stages of central settlement, the values of infiltration ratio were found to be lower than for the corresponding unreinforced case. This observed behavior of restraining cracks and an increase in limiting maximum distortion level was due primarily to the reinforcement effect of soil–fiber interaction.

For an unreinforced soil barrier, the magnitudes of the strain value corresponding to the limiting distortion level for 0.6 m and 1.2 m thick soil barriers were 1.01% and 1.73%, respectively; in comparison, for 0.6 m and 1.2 m thick soil barriers reinforced with polyester fibers, they were 1.31% and 3.4%, respectively. This implies that the FRSB has sustained higher strain values than the corresponding unreinforced soil barrier, at the onset of water breakthrough.

Figures 10a–10f show the status of the 0.6 m and 1.2 m thick soil barriers with and without two types of fiber at the end of the centrifuge test. A distinct and clear full penetration of the crack through the unreinforced soil barriers, even with an overburden equivalent to that of landfill covers, can be seen in Figures 10a and 10d. When the soil barrier was strengthened with 90 mm long polyester fibers, with a fiber content of 0.5%, a narrow crack extending up to its full depth was noticed (Figure 10e). However, when the polyester fibers were used in a 1.2 m thick soil barrier, only tiny surface cracks were observed (Figure 10c). Identical behavior was observed for the 1.2 m thick soil barrier reinforced with 90 mm long polypropylene fibers at a fiber content of 0.5% (Figure 10b). From Figure 10f, it can be seen that the 0.6 m thick soil barrier reinforced with polypropylene fibers has not shown a distinct full-depth crack; however, interconnected fine cracks extending up to full depth were noticed. This could be the reason for the observation of a gradual increase in infiltration ratio at $a/l_{\text{lim}} = 0.107$ ($a = 0.43$ m) This observed behavior could be due to the reduced magnitude of the overburden pressure induced on the soil barrier. The performance of both thicknesses of FRSB was found to be much better than that of the corresponding unreinforced soil barriers. The reason for the formation of narrow and full penetration of cracks in the 0.6 m thick FRSB could be inadequate mobilization of the required tensile load to suppress cracking at the onset of differential settlement.

The length of the fibers is an important parameter. If short fibers are used, they may not be able to bridge the gaps in the cracked soil mass, and there is a chance that FRSB will be ineffective. Viswanadham *et al.* (2010b) reported that lower values of strain at crack initiation were reported for soil beams reinforced with 30 mm long polypropylene tape fibers at 0.5% fiber content than soil for beams reinforced with 90 mm long fibers at an identical fiber content. They reported that model soil barrier material compacted at its maximum dry unit

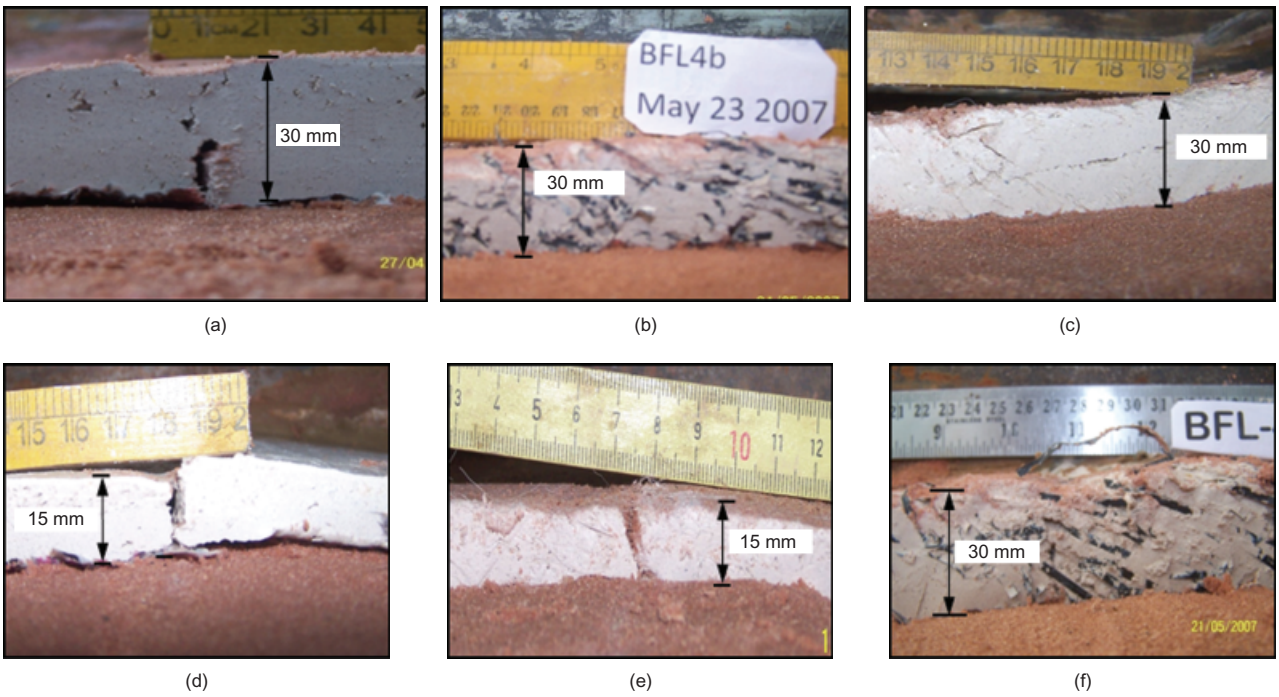

Figure 10. Status of soil barriers at zone of maximum curvature after inducing $a_{\text{max}} = 25$ mm: (a) Model BFL5r; (b) Model BFL4B; (c) Model BFL4C; (d) Model BFL8; (e) Model BFL4D; (f) Model BFL4A

weight and molding water content towards wet side of optimum (standard Proctor compaction) had a tensile strain at initiation of cracking of 1.09%. For the same soil, the incorporation of 0.5% and 90 mm long polypropylene fibers resulted in a strain at crack initiation of 2.27%, which is 2.1 times better than for an unreinforced soil beam. The observed deformation behavior of clay-based landfill covers was found to be in good agreement with the results reported by Viswanadham *et al.* (2010b). This was also found to be evident from the state of fibers (especially polypropylene tape fibers) exhumed from the soil barriers during post-test investigations. They were found to be distorted and split intermittently, which is a clear indication of their participation in restraining cracks.

6.2. Influence of geofiber type

Two types of geofibers were used in the present study, as explained in the preceding sections: polypropylene tape fibers and polyester fibers. Polypropylene fibers are very light in weight, and it was simple to prepare a uniform soil–fiber mix. There is less chance of accumulation of polypropylene fibers to form a cluster in one place within the soil matrix than there is for polyester fibers. The large specific gravity of polyester fibers implies low fiber volume and a lower number of fibers, and may lead to a tendency to premature water-breakthrough in soil barriers at the onset of differential settlement. As shown in Table 2, the specific gravity of polyester fibers is 1.334 and that of polypropylene fibers is 0.91. However, the two fibers were found to have different equivalent diameters. Based on the tests carried out so far, a distinct influence of fiber type on the deformation behavior of soil barriers could not be ascertained. This could be attributed to the availability of large surface areas of fibers to interact with the soil in the case of polypropylene tape fibers. The denier of polypropylene tape fibers was found to be about 75 times more than that of the polyester fibers used in the present study.

From these results, it is clear that if a landfill cover with 0.6 m thick soil barrier experiences a distortion level greater than or equal to 0.05, then it has a tendency to experience cracking sufficient to lose its integrity. Similarly, for a landfill cover with a 1.2 m thick soil barrier, the limiting distortion level is about 0.083 with full-penetration cracking. Although a delay in water breakthrough was observed for a 1.2 m thick clay-based landfill cover, distinct full-depth cracking was observed. Hence there is a need to evolve options for the strengthening of soil barriers of landfill covers to enhance their sealing efficiency, even at the onset of large differential settlements. One of the reasons for the superior performance of 1.2 m thick soil barriers reinforced with discrete fiber reinforcement over the respective 0.6 m thick case may be an increase in the initial stresses within the barrier. This results in an increase in confining stresses, which in turn enhances bond stresses along the soil/fiber interfaces. From the present study, geofiber-reinforced soil barriers 1.2 m thick (especially with a fiber content of 0.5% and fiber length of 90 mm) were found to be very effective in restraining cracking and in enhancing the water breakthrough capacity. However, it is very important to achieve uniform blending of fibers with soil in the field. Some of the field mixing methods adopted by Zhang *et al.* (2003) and Fowmes *et al.* (2006) can be thought as viable options. Hence the resulting experience of using the discrete and randomly distributed fiber reinforcement technique remains very interesting, and calls for more field trials. To some extent, this can be realized in repairing distressed landfill covers by replacing at least top 50% thickness with the same soil blended with fibers.

7. CONCLUSIONS

In this paper, the performance of moist-compacted clay-based landfill covers with and without discrete and randomly distributed geofibers at the onset of differential settlement was demonstrated by performing centrifuge tests at 40*g*. A hydraulic-based differential settlement simulator was used for simulating the differential settlement of landfill covers during centrifuge tests. Two thickness of soil barrier (0.6 m and 1.2 m) and two types of fiber were varied by maintaining: (1) the fiber content and length of fibers; and (2) identical type of the soil barrier material and moist-compacted state of the soil barrier material of landfill covers. The deduced scaling considerations imply that fiber dimensions need to be identical in a centrifuge model and prototype and be treated as discrete inclusions, analogous to other admixtures such as lime and cement.

Based on analysis and interpretation of the centrifuge test results, the following conclusions are drawn.

1. Centrifuge model tests on 0.6 m and 1.2 m thick unreinforced soil barriers with an overburden equivalent to that of landfill covers was found to experience a crack of narrow width extending up to full depth of the soil barrier. Catastrophic water breakthrough was observed for a 0.6 m thick unreinforced clay-based landfill cover at a settlement ratio of 0.56 and distortion level of 0.069. In comparison, a 1.2 m thick unreinforced soil barrier with an overburden equivalent to that of landfill covers was found to sustain a large distortion level. The limiting distortion level corresponding to water breakthrough was found to be 0.083 at a settlement ratio of 0.66. Water breakthrough was delayed in the case of the 1.2 m thick barrier, compared with the 0.6 m thick barrier. The maximum outer fiber strain for a thin soil barrier was less than for a thick barrier for all settlement stages. This indicates that a thicker barrier can withstand greater deformations, maintaining the sealing efficiency.
2. The deformation behavior of 0.6 m thick fiber-reinforced soil barrier subjected to an overburden equivalent to that of landfill covers was found to be superior to that of the corresponding unreinforced soil barrier. The limiting distortion levels for polypropylene tape fiber-reinforced and polyester fiber-reinforced soil barriers of 0.6 m thickness were registered as 0.071 and 0.081, which is 1.2–1.3

times that of the corresponding unreinforced soil barrier. The values of infiltration ratio were found to be on the higher side for the 0.6 m thick soil barrier without any fiber reinforcement throughout all stages of the test. Hence a fiber-reinforced soil barrier is very efficient when compared with an unreinforced barrier of identical thickness.

3. The 1.2 m thick soil barriers reinforced with polypropylene tape and polyester fiber and subjected to 25 kN/m^2 were found to have tiny surface cracks, and to sustain their integrity even after being subjected to a distortion level of 0.125. This implies that the fiber-reinforced soil barrier has sustained higher strain values than the corresponding unreinforced soil barrier, at the onset of water breakthrough.
4. A distinct influence of fiber type on the deformation behavior of soil barriers could not be ascertained, although polypropylene fibers are light in weight, and hence there is a chance of a greater number of fibers in a given volume of soil than for polyester fibers. To a large extent this was compensated by the availability of large surface areas of polypropylene tape fibers, which might have resulted in mobilization of bond stresses along the soil/fiber interface. For the types of fiber used in the present study, blending of 0.5% by dry weight of soil with 90 mm long fibers was found to be effective in improving the integrity and water breakthrough tendency of clay-based landfill covers subjected to differential settlements.

Recently, Moon *et al.* (2008) reported that the gas permeability of a soil barrier was about two or three orders of magnitude greater than permeability to water. In this case, it is questionable whether the compacted soil barrier subjected to bending will be effective in preventing gas emissions from landfill sites, although a 1.2 m thick unreinforced soil barrier subjected to an overburden equivalent to that of landfill covers appear to sustain slightly larger distortion, and the occurrence of full-penetration cracking is an issue, which may affect its performance. In such situations, the use of discrete and randomly distributed geofiber reinforcement inclusions within the soil barrier can enhance the performance of clay-based landfill covers. However, further work in this direction is warranted to understand the efficacy of soil barriers subjected to differential settlements in preventing gas emissions from landfill sites.

ACKNOWLEDGEMENTS

This research was supported by the Indo-French Collaboration for Advanced Research (IFCPAR), and their support is greatly acknowledged. The writers thank the staff at the National Geotechnical Centrifuge Facility (NGCF), Indian Institute of Technology Bombay, Powai, Mumbai 400 076, for their active involvement during the course of the study. The writers would also like to thank M/s Reliance Industries Limited, Mumbai, India, and M/s Techfab (India) for supplying fibers used in the present study.

NOTATIONS

Basic SI units are given in parentheses.

A	cross-sectional area of fiber (m^2)
A'	surface area along fiber (m^2)
a	central settlement (m)
a_{max}	maximum central settlement (m)
a/a_{max}	settlement ratio (dimensionless)
a/l	distortion level (dimensionless)
$(a/l)_{lim}$	limiting distortion level (dimensionless)
c'	effective cohesion (N/m^2)
d	thickness of soil barrier (m)
b	fiber width (m)
E	elastic modulus of fiber (Pa)
E_{50}	elastic modulus of soil barrier material (Pa)
g	acceleration due to gravity (m/s^2)
l	influence length (m)
l'	fiber length (m)
N	scale factor (dimensionless)
R	radius of curvature (m)
s_r	settlement rate in model dimensions (m/s)
t	thickness of fiber (m)
V_a	volume of water at required central settlement (m^3)
V_0	initial volume of water (m^3)
$w(x)$	deformation of soil barrier (m)
x	horizontal distance from center of soil barrier (m)
ε_{of}	outer fiber strain (dimensionless)
ε_t	tensile strain of fiber (dimensionless)
σ_t	tensile strength of the fiber (Pa)
σ_o	overburden pressure (Pa)
τ_b	bond strength of fiber (Pa)
ϕ'	effective angle of internal friction (degrees)

ABBREVIATIONS

CSB	compacted soil barrier
DRDF	discrete and randomly distributed fiber reinforcement
FRSB	fiber-reinforced soil barrier
GCL	geosynthetic clay liner
PPT	pore pressure transducer
USCS	Unified Soil Classification System

REFERENCES

ADEME-LIRIGM (2005). *Guide méthodologique pour le suivi des tassements des centres de stockage de déchets de classe II*. Guide méthodologique de l' ADEME (in French).

Benson, C. H., Daniel, D. E. & Boutwell, G. P. (1999). Field performance of compacted clay liners. *Journal of Geotechnical and Geoenvironmental Engineering, ASCE*, **126**, No. 5, 390–403.

Bredariol, A. W., Martin, J. P., Cheng, S. & Tull, C. F. (1995). Flexural cracking of compacted clay in landfill covers. *Geoenvironment 2000*, Geotechnical Special Publication 46, Acar, Y. B. & Daniel, D. E., Editors, ASCE, Reston, VA, pp. 914–931.

Camp, S., Ple, O. & Gourc, J. P. (2009). Proposed protocol for

characterizing a clay layer subjected to bending. *Geotechnical Testing Journal, ASTM*, **32**, No. 3, 273–279.

Consoli, N. C., Vendruscolo, M. A., Fonini, A. & Rosa, F.D. (2010). Fiber reinforcement effects on sand considering a wide cementation range. *Geotextiles and Geomembranes*, **27**, No. 3, 196–203.

Consoli, N. C., de Moraes, R. R. & Festugato, L. (2011). Split tensile strength of monofilament polypropylene fiber-reinforced cemented sandy soils. *Geosynthetics International*, **18**, No. 2, 57–62.

Das, A., Jayashree, Ch. & Viswanadham, B. V. S. (2009). Effect of randomly distributed geofibers on the piping behaviour of embankments constructed with fly ash as a fill material. *Geotextiles and Geomembranes*, **27**, No. 5, 341–349.

Edelmann, L., Hertweck, M. & Amman, P. (1999). Mechanical behaviour of landfill barrier systems. *Proceedings of the Institution of Civil Engineers, Geotechnical Engineering*, **137**, No. 4, 215–223.

Falorca, I. M. C. F. G. & Pinto, M. I. M. (2011). Effect of short, randomly distributed, polypropylene microfibres on shear strength behaviour of soils. *Geosynthetics International*, **18**, No. 1, 2–11.

Fowmes, G. J., Dixon, N. & Jones, D. R. V. (2006). Use of randomly reinforced soils in barrier systems. *Proceedings of the 5th International Congress on Environmental Geotechnics*, Thomas, H. R., Editor, Thomas Telford (Publisher), London, Vol. 2, pp. 709–716.

Gourc, J. P., Camp, S., Viswanadham, B. V. S. & Rajesh, S. (2010a). Deformation behaviour of clay cap barriers of hazardous waste containment systems: full-scale and centrifuge tests. *Geotextiles and Geomembranes*, **28**, No. 3, 281–291.

Gourc, J. P., Staub, M. J. & Conte, M. (2010b). Decoupling MSW settlement into mechanical and biochemical processes: modelling and validation on large-scale setups. *Waste Management*, **30**, No. 8–9, 1556–1568.

GRAM++ (2004). *Technical document*, CSRE, Indian Institute of Technology Bombay. http://www.csre.iitb.ac.in/gram++/.

Gucunski, N., Ganji, V. & Maher, M. H. (1996). Analysis of settlements of landfill caps by fem. *Proceedings of the 3rd International Symposium on Environmental Geotechnology*, Fang, H. Y. & Inyang, H. I., Editors, Vol. 1, pp. 485–494.

Heerten, G. & Koerner, R. (2008). Cover systems for landfills and brownfields. *Proceedings of the 24th SKZ-Fachtagung Die Sichere Deponie*, Wurzburg, Germany, pp. 1–25.

Izawa, J., Ito, H., Saito, T., Ueno, M. & Kuwano, I. (2009). Development of rational seismic design method for geogrid-reinforced soil wall combined with fiber-mixed soil-cement and its applications. *Geosynthetics International*, **16**, No. 4, 286–310.

Jessberger, H. L. & Stone, K. J. L. (1991). Subsidence effect on clay barriers. *Géotechnique*, **41**, No. 2, 185–194.

Keck, K. N. & Seitz, R. R. (2002). *Potential for Subsidence at the Low-Level Radioactive Waste Disposal Area*. INEEL/EXT-02–01154, Idaho National Engineering and Environmental Laboratory, US Department of Energy.

LaGatta, M. D., Boardman, B. T., Cooley, B. H. & Daniel, D. E. (1997). Geosynthetic clay liners subjected to differential settlement. *Journal of Geotechnical and Geoenvironmental Engineering, ASCE*, **123**, No. 5, 402–410.

Lee, K. L. & Shen, C. K. (1969). Horizontal movements related to subsidence. *Journal of Soil Mechanics and Foundations Division, ASCE*, **94**, No. 6, 139–166.

Li, G. X., Jie, Y. X. & Jie, G. Z. (2001). Study on the critical height of fiber-reinforced slope by centrifuge test. *Proceedings of Landmarks in Earth Reinforcement*, Ochiai, H., Otani, J., Yasufuku, N. & Omine, K., Editors, Swets and Zeitlinger, The Netherlands, Vol. 1, pp. 239–241.

Liang, R.Y., Lommler, J. C., Lee, S. & Meyers, B. (1994). Case studies: clay cover cracking analysis using FEM techniques, *Fracture Mechanics Applied to Geotechnical Engineering*, Vallejo, L. E. & Liang, R. Y., Editors, Geotechnical Special Publication No. 43, ASCE, Reston, VA, pp. 86–101.

Lovisa, J., Shukla, S. K. & Sivakugan, N. (2010). Shear strength of randomly distributed moist fibre-reinforced sand. *Geosynthetics International*, **17**, No. 2, 100–106.

Maher, M. H. & Gray, D. H. (1990). Static response of sand reinforced with randomly distributed fibers. *Journal of Geotechnical Engineering*, **116**, No. 11, 1661–1677.

Maher, M. H. & Ho, Y. C. (1994). Mechanical properties of kaolinite/fiber soil composite. *Journal of Geotechnical Engineering*, ASCE, **120**, No. 8, 1381–1393.

Miller, C. J. & Rifai, S. (2004). Fiber reinforcement for waste containment soil liners. *Journal of Environmental Engineering, ASCE*, **130**, No. 8, 891–895.

Moon, S., Nam, K., Kim, J. Y., Hwan, S. K. & Chung, M. (2008). Effectiveness of compacted soil liner as a gas barrier layer in the landfill cover system. *Waste management*, **28**, No. 10, 1909–1914.

Morel, J. C. & Gourc, J. P. (1997). Mechanical behaviour of sand reinforced with mesh elements. *Geosynthetics International*, **4**, No. 5, 481–508.

Nataraj, M. S. & McManis, K. L. (1997). Strength and deformation properties of soils reinforced with fibrillated fibers. *Geosynthetics International*, **4**, No. 1, 65–79.

Park, S.-S. (2009). Effect of fiber reinforcement and distribution on unconfined compressive strength of fiber-reinforced cemented sand. *Geotextiles and Geomembranes*, **27**, No. 2, 162–166.

Qian, X., Koerner, R. M. & Gray, D. H. (2002). *Geotechnical Aspects of Landfill Design and Construction*, 1st edition, Prentice Hall, Englewood Cliffs, NJ.

Rajesh, S. & Viswanadham, B. V. S. (2011). Hydro-mechanical behavior of geogrid reinforced soil barriers of landfill cover systems. *Geotextiles and Geomembranes*, **29**, No. 1, 51–64.

Ranjan, G., Vasan, R. M. & Charan, H. D. (1994). Behaviour of plastic-fiber-reinforced sand. *Geotextiles and Geomembranes*, **13**, No. 8, 555–565.

Rodatz, W. & Oltmanns, W. (1997). Permeability and stress–strain behaviour of fiber-reinforced soils for landfill liners systems. *Advanced landfill liner systems*, August, H., Holzloner, U. & Meggyes, T., Editors, Thomas Telford, London, pp. 321–332.

Sagaseta, C. (1987). Analysis of undrained soil deformation due to ground loss. *Géotechnique*, **37**, No. 3, 301–320.

Santoni, R. L., Tingle, J. S. & Webster, S. L. (2001). Engineering properties of sand-fiber mixtures for road construction. *Journal of Geotechnical and Geoenvironmental Engineering, ASCE*, **127**, No. 3, 258–268.

Scherbeck, R. & Jessberger, H. L. (1993). Assessment of deformed mineral sealing layers. Waste disposal by landfill. *Proceedings of the Symposium Green '93, Geotechnics Related to the Environment*, Sarsby, R. W., Editor, A. A. Balkema, Rotterdam, pp. 477–486.

Sengupta, S. S. (2005). *Modelling deformation behaviour of compacted soil liners in a geotechnical centrifuge*. MTech dissertation, Indian Institute of Technology Bombay, India.

Staub, M. J., Laurent, J. P., Gourc, J. P. & Morra, C. (2010). Applicability of time domain reflectometry water content measurements in municipal solid waste. *Vadose Zone Journal*, **9**, No. 1, 160–171.

Staub, M., Marcolina, G., Gourc, J. P. & Simonin, R. (2011). An incremental model to assess the environmental impact of cap cover systems on MSW landfill emissions. *Geotextiles and Geomembranes*, **29**, No. 3, 298–312.

Tang, C. S., Shi, B., Gao, W., Chen, F. & Cai, Yi. (2007). Strength and mechanical behaviour of short polypropylene fiber reinforced and cement stabilised clayey soil. *Geotextiles and Geomembranes*, **25**, No. 3, 194–202.

Tang, C. S, Shi, B. & Zhao, L.-Z. (2010). Interfacial shear strength of fiber reinforced soil. *Geotextiles and Geomembranes*, **28**, No. 1, 54–62.

Taylor, G. D. (1983). *Material of Construction*, 2nd, Edition, Construction Press, London, pp. 292–300.

Tognon, A. R., Rowe, R. K. & Moore, I. D. (2000). Geomembrane strain observed in large-scale testing of protection layers. *Journal of Geotechnical and Geoenvironmental Engineering, ASCE*, **126**, No. 12, 1194–1208.

Viswanadham, B. V. S. & Muthukumaran, A. E. (2007). Influence of geogrid layer on the integrity of compacted clay liners of landfills. *Soils and Foundations*, **47**, No. 3, 519–534.

Viswanadham, B. V. S. & Rajesh, S. (2009). Centrifuge model tests on

clay based engineered barriers subjected to differential settlements. *Applied Clay Science*, **42**, No. 3–4, 460–472.

Viswanadham, B. V. S., Jha, B. K. & Sengupta, S. S. (2009). Centrifuge testing of fiber reinforced soil liners for waste containment systems. *Journal of Practice Periodical of Hazardous, Toxic, and Radioactive Waste Management, ASCE*, **13**, No. 1, 45–58.

Viswanadham, B. V. S., Jha, B. K. & Pawar, S. N. (2010a). Experimental study on flexural testing of compacted soil beams. *Journal of Material in Civil Engineering, ASCE*, **22**, No. 5, 460–468.

Viswanadham, B. V. S., Jha, B. K. & Pawar, S. N. (2010b). Influence of geofibers on the flexural behaviour of compacted soil beams. *Geosynthetics International*, **17**, No. 2, 86–99.

Yetimoglu, T. & Salbas, O. (2003). A study on shear strength of sands reinforced with randomly distributed discrete fibers. *Geotextiles and Geomembranes*, **21**, No. 2, 103–100.

Zhang, Z., Farrag, K. & Morvant, M. (2003). *Evaluation of the Effect of Synthetic Fibers and Nonwoven Geotextile Reinforcement on the Stability of Heavy Clay Embankments*, FHWA/LA.03/373. Louisiana Transportation Research Center, Baton Rouge, LA, USA, pp. 7–19.

Ziegler, S., Leshchinsky, D., Ling, H. I. & Perry, E. B. (1998). Effect of short polymeric fibers on crack development in clays. *Soils and Foundations*, **38**, No. 1, 247–253.

Zornberg, J. G. (2005). Geosynthetic reinforcement in landfill design: US perspectives. *Proceedings, Geo-Frontiers 2005*, Geotechnical Special Publication 141 (CD-ROM), Zornberg, J. J., Gabr, M. & Bowders, J. J., Editors, ASCE, Reston, VA.

The Editor welcomes discussion on all papers published in Geosynthetics International. Please email your contribution to discussion@geosynthetics-international.com by 15 April 2012.